An Anatomical Atlas-Based Method for fNIRS Tomography

Yong Xu[1,2], PhD, Yaling Pei[2], PhD, and Randall L. Barbour[1,2], PhD

[1]State University of New York, Downstate Medical Center, Box 40, 450 Clarkson Avenue, Brooklyn, New York 11203,
[2]NIRx Medical Technologies LLC, 15 Cherry Lane, Glen Head, NY 11545

Introduction

For functional neuroimaging modalities, a capability that is increasingly regarded as essential is the ability to map image findings to the underlying anatomy. In the case of diffusion optical tomography (DOT) imaging, complicating the goal of mapping DOT activation findings to brain anatomy is the need for a representative altas that can support the flexible generation of the imaging operator for any selected optode arrangement. Whereas access to individual structural maps is increasingly common, efforts to generate individualized finite element method (FEM) meshes in support of DOT reconstruction can be burdensome. To facilitate the accurate generation and mapping of DOT findings, we have established a library of FEM meshes from a selected MRI atlas that has been segmented according to different tissue types. Specification of optode arrangement corresponding to individual or multiple head regions is made either by graphical selection, or through the loading of measures of head-shape and optode position followed by an affine transformation based on measured fiducials. This information is used to configure the corresponding imaging operators obtained from a precalculated database. Experimental evaluation has shown that determination of head shape, optode location, reconstruction of activation maps and mapping to individual atlases can be made with high fidelity.

Methods

MR-based FEM model library: A single-subject MRI of the brain, having a 1 mm resolution and obtained form Source Signal Imaging, was used as our atlas in the present study [1]. The image was segmented into five classes including skin, skull, cerebrospinal fluid, gray matter, and white matter. The FEM model library consists of the FEM meshes of brain regions of interest (ROIs) and corresponding forward solutions to the photon diffusion equation for identified tissues. Each ROI mesh is generated from the segmented image atlas by use of EMSE MR Viewer [1], in which there are nearly 3000 -3500 nodes, as shown in Fig. 1A. The spatial extent of each mesh file normally covers about 50-75 cm^2 on the surface of the head and has a depth of up to 5 cm. In order to cover all regions of brain, we have generated 25 overlapping ROI meshes in our library. Fig. 1B shows twelve ROI meshes of the library.

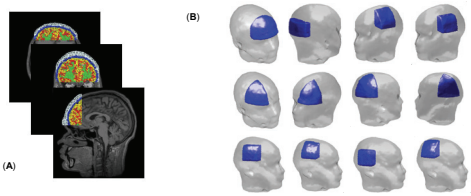

Figure 1. MRI-based segmented FEM brain mesh library.

In each ROI mesh there are about 400 boundary nodes on the surface of the head with approximately a 4 mm spatial resolution. We consider the surface nodes as the possible source/detector positions, and numerically solve the FEM discretized photon diffusion equations using Type III boundary conditions [2]:

$$[A]\{\Phi\} = \{b\}$$
$$[A]\{\partial\Phi/\partial\chi\} = \{\partial b/\partial\chi\} - [\partial A/\partial\chi]\{\Phi\}$$

Solutions to these equations {Φ} and {∂Φ/∂χ} provide the reference detector values and weight functions (Jacobian operators), respectively. The pre-calculated results are incorporated into the FEM model database. The complete brain FEM model database represents over 200 G bytes of data.

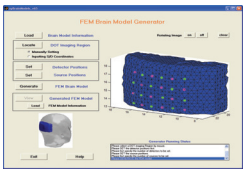

Figure 2. FEM Brain Model Generator.

To efficiently and conveniently employ the model library, we have developed a Matlab-based interactive FEM model generation tool: FEM Brain Model Generator, as shown in Figure 2. By using the generator, the users can easily generate themselves FEM brain models matching the experimental source/detector geometries by inputting the coordinates of source/detector positions and brain fiducial points measured by 3D digitizer, or by using the generator GUI to manually specify source and detector positions on the head surface of the image atlas.

3D Digitizing and registration: Mapping of optode-position information from an individual subject to an FEM library model, is accomplished by first digitizing brain fiducial points and source/detector positions and then applying an affine transformation. The fiducials and optode positions can be measured by a commercial 3D digitizer, e.g., Polhemus patriot, as shown in Figure 3A. Figure 3B illustrates thirteen 10-20 system points that are selected as the standard head shape fiducials in our method. The measured coordinates (P_f) of 13 fiducial points on individual subject head surface and the known coordinates (P_0) of 13 fiducial points on the image atlas surface are related by an affine transformation matrix (M) [3]:

$$P_0 = P_f M$$

Where

$$P_0 = \begin{bmatrix} x_1 & y_1 & z_1 & 1 \\ x_2 & y_2 & z_2 & 1 \\ \vdots & \vdots & \vdots & \vdots \\ x_{13} & y_{13} & z_{13} & 1 \end{bmatrix}, \quad P_f = \begin{bmatrix} x_{f1} & y_{f1} & z_{f1} & 1 \\ x_{f2} & y_{f2} & z_{f2} & 1 \\ \vdots & \vdots & \vdots & \vdots \\ x_{f13} & y_{f13} & z_{f13} & 1 \end{bmatrix}, \quad M = \begin{bmatrix} m_{11} & m_{12} & m_{13} & 0 \\ m_{21} & m_{22} & m_{23} & 0 \\ m_{31} & m_{32} & m_{33} & 0 \\ m_{41} & m_{42} & m_{43} & 1 \end{bmatrix}.$$

From the equation above, the affine transformation matrix M can be solved by a least square method using matrix left division:

$$M = P_f \backslash P_0$$

Next, the measured optode coordinates P_d are registered to the image atlas by following affine transformation:

$$P_i = P_d M$$

where P_i is the registered optode coordinate matrix.

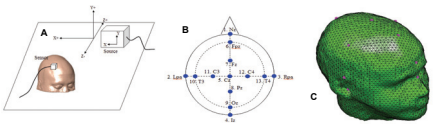

Figure 3. (A) 3D Digitizing; (B) Definition of fiducial points; (C) Image atlas and fiducial points (pink dots).

Image reconstruction: 3D images of the Hb signal were reconstructed by using the normalized difference method [4]. This method solves a modified linear perturbation equation that is robust to many of the uncertainties common to experimental studies including uncertainties associated with the initial guess, also known as the reference medium. Use of the linear approximately makes real-time 3D imaging feasible.

Anatomical labeling of fNIRS image: To support quantitative measures, we have registered the Automated Anatomical Labeling (AAL) brain atlas of SPM[5] to our image atlas by an affine transformation, as shown in Figure 4. This allows for the query of registered fNIRS images so as to identify specific brain regions. This information was used to explore the accuracy by which fNIRS images are mapped to our atlas.

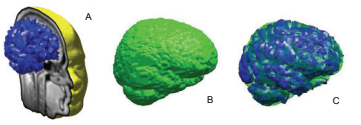

Figure 4. (A) Image atlas; (B) AAL brain atlas; (C) Registration of AAL brain onto image brain.

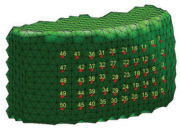

Figure 5. FEM mesh and source/detector configuration for simulation studies. The mesh has 4256 nodes and 18383 tetrahedral elements. 50Sx50D optode array covers 4x10 cm area.

Results

Spatial and temporal accuracies of 3D image mapping: By using numerical simulations, the spatial and temporal accuracies of image mapping are investiged. Conditions explored: as shown in Fig.5, optode array 50S x 50D covering 4 x 10 cm area, symmetric to midline. Inclusions: 1.5 cm object, mean depth 2 cm, inclusion 1 below source 28 and inclusion 2 below source 8. Initial Guess: μ_a=0.06, μ_s=10 cm^{-1}. Target Media (background): 1, μ_a=0.04; 2, 0.06; 3, 0.08; 4, 0.10; 5, 0.12; 6, 0.15 cm^{-1}; and medium 7 = medium 5 except inhomogenous background (CSF layer, 10% background). Noise Level[6]: 1, 1%-10%; 2, 2%-20%; 3, 3%-30%; 4, 5%-50%; and 5, 8%-80%. The distance between centers of target inclusion and reconstructed inclusion (50% max threshold) is selected as the measurement of spatial error, and the temporal correlation between target medium and reconstructed image as the temporal accuracy [6].

Figure 6 shows position of Inclusion 1, Panel A, reconstructed result for target medium 2, Panel B. Panel C: affine transformation to representative subject; Panel D, example of representative AAL finding. Findings support accurate mapping of image finding both to fNIRS image atlas and individual MR. The initial guess, inclusion contrast and noise dependences of spatial accuracy are presented in Figures 7~9, and the normalized modulation amplitude and noise dependences of temporal accuracy are shown in Figures 10~12. Table 1 shows AAL mapping results corresponding the blue curve in Fig.7 that explore the sensitivity of mapping accuracy on increasing errors in the intial guess. Listed values are percentage of total volume contained by indicated tissue types (50% max threshold). Results demonstrate good fidelity to increasing errors in initial guess.

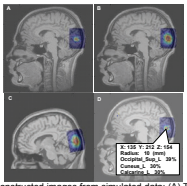

Figure 6. Reconstructed images from simulated data: (A) Target; (B) Reconstructed image; (C) Registered image; (D) Anatomical labeling.

Table 1. Anatomical labels and percentages per cluster in reconstructed inclusion region for four target media

		Target Medium (%)						
Label	Ideal (%)	1	2	3	4	5	6	7
Cuneus_L	51	49	52	51	50	50	48	46
Calcarine_L	25	25	24	23	24	25	23	27
Cuneus_R	13	14	12	13	14	14	17	14
Occipital_Sup_L	8	11	11	10	10	9	9	9
(others)	3	1	1	3	2	2	3	4

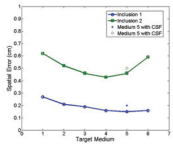

Figure 7. Target medium dependence of spatial accuracy for noise-free data, where the inclusion contrast is 2.0.

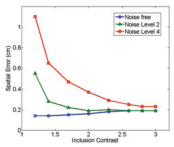

Figure 8. Contrast dependence of spatial accuracy for inclusion 1 with target medium 4 .

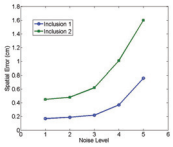

Figure 9. Noise level dependence of spatial accuracy for target medium 4. Where the inclusion contrast is 2.0.

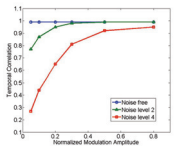

Figure 10. Modulation amplitude dependence of temporal accuracy for inclusion 1 with target medium 4.

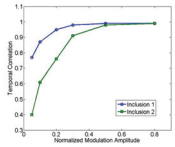

Figure 11. Comparison of modulation amplitude dependences of temporal accuracy for inclusions 1 and 2 with target medium 4. where the noise level is 2.

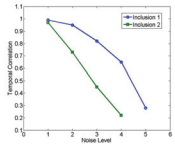

Figure 12. Noise level dependence of temporal accuracy for target medium 4. Where the normalized modulation amplitude is 0.2.

Experimental Validation with Programmable Anthropomorphic Head Phantom: Results in Figure 13 show image overlay obtained from frontal cortex study on head phantom containing programmable electrochormic cell to mimic hemoglobin signal [7]. The 1.2x1.2x0.2 (cm^3) cell is embeded in right frontal brain to a depth of ~2 cm below the head surface. Positionally error of highest contrast pixel is < 3mm. Figure 14 shows result of Fourier Transform for programmed and recovered function.

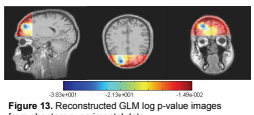

Figure 13. Reconstructed GLM log p-value images from phantom experimental data.

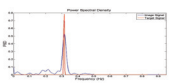

Figure 14. Power spectral density distributions of LC cell driven signal (red) and reconstructed signal (blue).

Conclusions

In summary, we have developed an anatomical atlas-based method for efficient generation and registration of 3D DOT image findings. As confirmed by numerical simulations and experimental data from solid-state programmable phantoms, our method is computation-efficient and is able to carry out, with high spatial and temporal accuracies, the necessary mappings—of optode-position information from an individual subject to an FEM library model, and of volumetric image information from the model back to the individual.

The reported capabilities have been integrated into our NAVI computing environment [8] to support the model-based fNIRS reconstruction and generation of MR-based montages. Recently, the described methodology has been applied to human brain visual activation studies [9].

References

[1] http://www.sourcesignal.com
[2] K. D. Paulsen and H. Jiang, "Spatially-varying optical property reconstruction using a finite element diffusion equation approximation," *Med. Phys.*, vol. 22, pp. 691–702, 1995.
[3] A. K. Singh, M. Okamoto, et. al., "Spatial registration of multichannel multi-subject fNIRS data to MNI space without MRI," *NeuroImage*, 27, 842-851, 2005.
[4] Y. Pei, H.L. Graber, and R.L. Barbour, " Influence of systematic errors in reference states on image quality and on stability of derived information for dc optical imaging", *Applied Optics*, vol. 40, pp. 5755–5769, 2001.
[5] N. Tzourio-Mazoyer, B. Landeau, et. al., "Automated Anatomical Labeling og Activations in SPM Using a Macroscopic Anatomical Parcellation of the MNI MRI Single-Subject Brain," NeuroImage, 15, 273-289, 2002.
[6] Y. Xu, Y. Pei, H. L. Graber, and R. L. Barbour, "Image quality improvement via spatial deconvolution in optical tomography: time-series imaging," J. Biomed. Opt. **10,** 051701 (2005).
[7] R.L. Barbour, R. Ansari, R. Al abdi, et. al., "Validation of near infrared spectroscopic (NIRS) imaging using programmable phantoms," *Proceedings of SPIE, Vol. 6870*, R.J. Nordstrom, Ed. (2008).
[8] Y. Pei, Y. Xu, and R.L. Barbour, "NAVI-SciPort solution: A problem solving environment (PSE) for NIRS data analysis," Poster No. 221 M-AM at Human Brain Mapping 2007 (Chicago, IL, June 10-14, 2007).
[9] G.R.Wylie, H.L.Graber, G.T.Voelbel, et. al., "Using co-variations in the Hb signal to detect visual activation: A near infrared spectroscopic imaging study", *NeuroImage*, vol. 47, pp. 473-481, 2009.

This work was supported under grant nos. 1R41NS050007-01, 1R42NS050007-02, 2R44NS049734-02, and DARPA-BAA-09-27.